Bioactive Materials 37 (2024) 424–438

Contents lists available at ScienceDirect

Bioactive Materials

journal homepage: www.keaipublishing.com/en/journals/bioactive-materials

Regulation of metabolic microenvironment with a nanocomposite hydrogel for improved bone fracture healing

Kangkang Zha [a,b,1], Meijun Tan [c,1], Yiqiang Hu [a,b,1], Weixian Hu [a,b,1], Shengming Zhang [a,b], Yanzhi Zhao [a,b], Ze Lin [a,b], Wenqian Zhang [a,b], Hang Xue [a,b], Bobin Mi [a,b], Wu Zhou [a,b,**], Qian Feng [c,***], Faqi Cao [a,b,****], Guohui Liu [a,b,*]

[a] Department of Orthopeadics, Union Hospital, Tongji Medical College, Huazhong University of Science and Technology, Wuhan, 430022, China
[b] Hubei Province Key Laboratory of Oral and Maxillofacial Development and Regeneration, Wuhan, 430022, China
[c] Key Laboratory of Biorheological Science and Technology, Ministry of Education, College of Bioengineering, Chongqing University, Chongqing, 400044, China

ARTICLE INFO

Keywords:
Bone fracture
Metabolic microenvironment
Macrophage
BMSC
Hydrogel

ABSTRACT

Bone nonunion poses an urgent clinical challenge that needs to be addressed. Recent studies have revealed that the metabolic microenvironment plays a vital role in fracture healing. Macrophages and bone marrow-derived mesenchymal stromal cells (BMSCs) are important targets for therapeutic interventions in bone fractures. Itaconate is a TCA cycle metabolite that has emerged as a potent macrophage immunomodulator that limits the inflammatory response. During osteogenic differentiation, BMSCs tend to undergo aerobic glycolysis and metabolize glucose to lactate. Copper ion (Cu^{2+}) is an essential trace element that participates in glucose metabolism and may stimulate glycolysis in BMSCs and promote osteogenesis. In this study, we develop a 4-octyl itaconate (4-OI)@Cu@Gel nanocomposite hydrogel that can effectively deliver and release 4-OI and Cu^{2+} to modulate the metabolic microenvironment and improve the functions of cells involved in the fracture healing process. The findings reveal that burst release of 4-OI reduces the inflammatory response, promotes M2 macrophage polarization, and alleviates oxidative stress, while sustained release of Cu^{2+} stimulates BMSC glycolysis and osteogenic differentiation and enhances endothelial cell angiogenesis. Consequently, the 4-OI@Cu@Gel system achieves rapid fracture healing in mice. Thus, this study proposes a promising regenerative strategy to expedite bone fracture healing through metabolic reprogramming of macrophages and BMSCs.

1. Introduction

As a result of rapid advancements in transportation and population aging, the incidence of fractures has gradually increased [1]. Delayed healing or bone nonunion affects approximately 5–10% of fracture patients, leading to adverse effects on their health, quality of life, and society's economic well-being [2]. Therefore, it is imperative to investigate approaches that expedite fracture healing and avert complications. Fracture healing is a highly intricate process that entails complex cellular and molecular interactions [3]. Mounting evidence indicates that these cells undergo metabolic adaptation under limited local nutrient availability and modulate their cellular functions during fracture healing [4]. The regulation of the metabolic microenvironment conducive to tissue regeneration represents an approach for treating bone fractures.

Prolonged inflammatory conditions within the fracture zone can

Peer review under responsibility of KeAi Communications Co., Ltd.

* Corresponding author. Department of Orthopeadics, Union Hospital, Tongji Medical College, Huazhong University of Science and Technology, Wuhan, 430022, China.

** Corresponding author. Department of Orthopeadics, Union Hospital, Tongji Medical College, Huazhong University of Science and Technology, Wuhan, 430022, China.

*** Corresponding author.

**** Corresponding author. Department of Orthopeadics, Union Hospital, Tongji Medical College, Huazhong University of Science and Technology, Wuhan, 430022, China.

E-mail addresses: 2016XH0120@hust.edu.cn (W. Zhou), qianfeng@cqu.edu.cn (Q. Feng), 13971293030@163.com (F. Cao), liuguohui@hust.edu.cn (G. Liu).

[1] These authors contributed equally to this work.

https://doi.org/10.1016/j.bioactmat.2024.03.025
Received 23 January 2024; Received in revised form 16 March 2024; Accepted 16 March 2024

impair bone healing [5]. Macrophages are important targets for the regulation of the local inflammatory response at the early stage of fracture healing. Upon exposure to inflammatory stimuli, macrophages undergo metabolic reprogramming to facilitate inflammatory responses by enhancing phagocytic function and cytokine release. The tricarboxylic acid (TCA) cycle in macrophages is tightly related to their phenotype and function [6]. Itaconate, a TCA cycle metabolite, is derived from *cis*-aconitate by the mitochondrial enzyme *cis*-aconitate decarboxylase (ACOD1) [7]. A disturbance in the TCA cycle in activated macrophages leads to the accumulation of itaconate, which exerts anti-inflammatory effects by suppressing succinate dehydrogenase, activating anti-inflammatory transcription factors, including nuclear factor erythroid 2-related factor 2 (Nrf2) and activating transcription factor 3 (ATF3), and inhibiting the NOD-like receptor thermal protein domain associated protein 3 (NLRP3) inflammasome [8]. Itaconate has emerged as a potent immunomodulator that limits the inflammatory response [9]. Thus, regulating the itaconate concentration in macrophages may be an efficient approach for alleviating the inflammatory response at the early stage of fracture healing.

Copper ion (Cu^{2+}) is an important trace element that has been applied to stimulate angiogenesis in the treatment of fractures and bone defects [10,11]. In addition, Cu^{2+} participates in the multiple cellular metabolism, including lipids and glucose [12]. Recent evidence suggests that glucose metabolism is a prominent metabolic feature of bone marrow-derived mesenchymal stromal cells (BMSCs), which tend to undergo aerobic glycolysis and metabolize glucose to lactate during osteogenic differentiation [13–15]. The hypoxia-inducible factor-1α (HIF-1α)-glucose transporter type 1 (GLUT1) signaling pathway is considered an important regulator of aerobic glycolysis [16,17]. It has been demonstrated that knockdown of HIF-1α results in suppressed osteogenesis [18]. The effect of Cu^{2+} on the expression of HIF-1α has been verified [19,20], but whether Cu^{2+} can induce the activation of the HIF-1α-GLUT1 signaling pathway and promote osteogenesis has not been determined.

In recent years, the application of bioactive materials has emerged as a promising approach for modulating the microenvironment and promoting bone fracture healing [21]. Covalent organic frameworks (COFs) are emerging crystalline porous organic polymers for the sustained delivery of drugs [22]. For example, Bhunia et al. fabricated a boronate-based COF loaded with dexamethasone and demonstrated that the hydrolytically stable COF nanocomposite was able to induce MSC osteogenic differentiation in the absence of an osteoinductive agent [23]. Hydrogels are widely applied in bone tissue engineering for cell adhesion and drug delivery due to their controllable mechanical properties, superior biocompatibility, and excellent drug loading capacity [24,25]. Hydrogel-based bone tissue engineering is an effective approach for treating bone fractures [26,27]. Thus, developing a drug delivery system based on COFs and hydrogels to modulate the local microenvironment and promote tissue regeneration represents a promising strategy to enhance fracture healing.

In this study, to enhance fracture healing and tissue regeneration, we designed a bioactive hydrogel encapsulated with 4-octyl itaconate (4-OI) (an itaconate derivative) and Cu COF. The burst release of 4-OI was hypothesized to alleviate the inflammatory response and oxidative stress to protect cells, while the sustained release of Cu^{2+} was hypothesized to improve bone regeneration and vessel formation. The effects of the

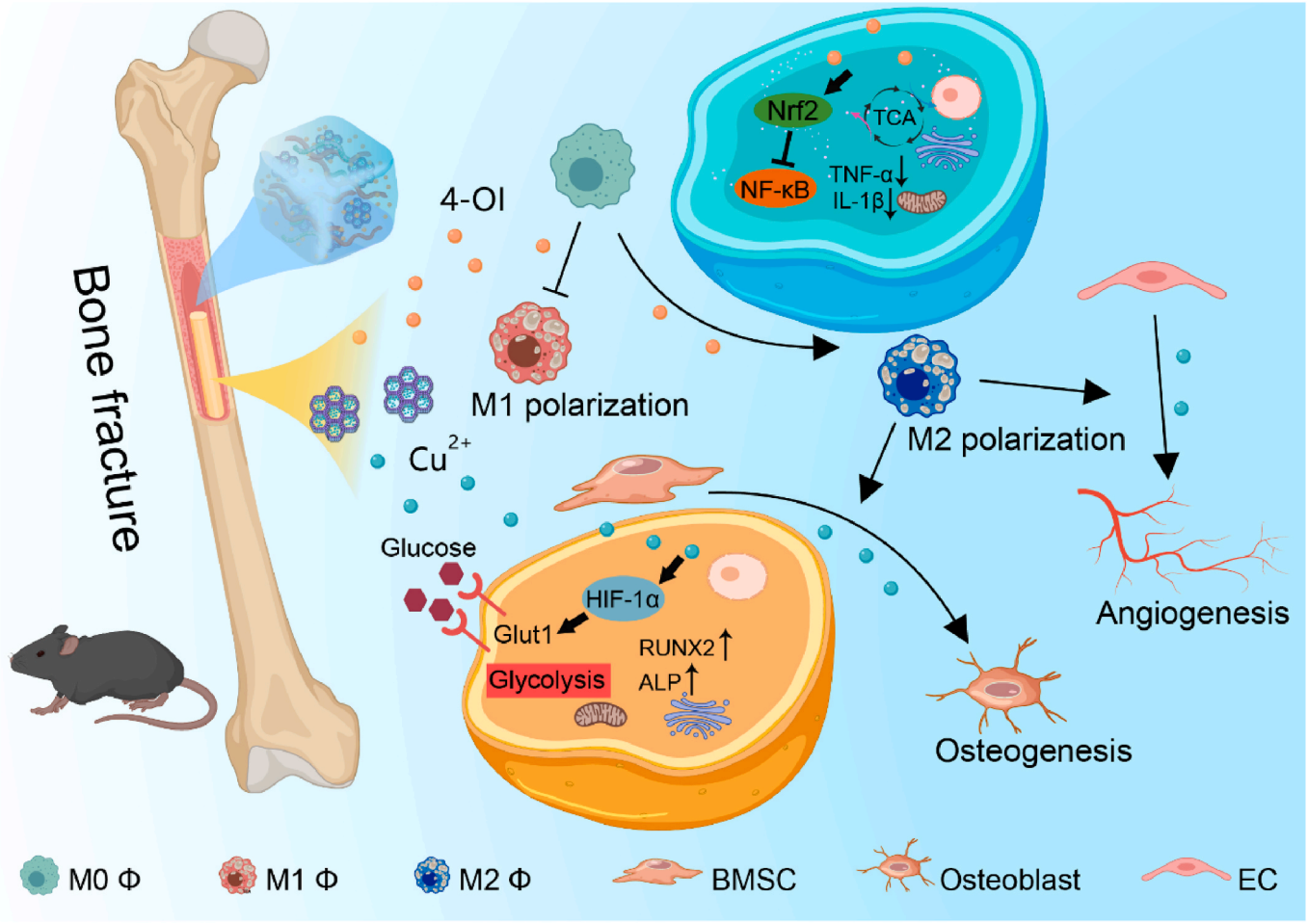

Fig. 1. Schematic diagram of the application of 4-OI@Cu@Gel for the regulation of bone metabolic microenvironment and fracture healing.

hydrogels on the activities of bone repair-related cells, including macrophages, BMSCs and endothelial cells, as well as the underlying molecular events, were investigated *in vitro*. In addition, we used a femur fracture mouse model to evaluate the *in vivo* efficacy of the composite hydrogel on fracture healing. The 4-OI@Cu@Gel hydrogel is expected to provide a new and effective treatment strategy for clinical bone nonunion (Fig. 1).

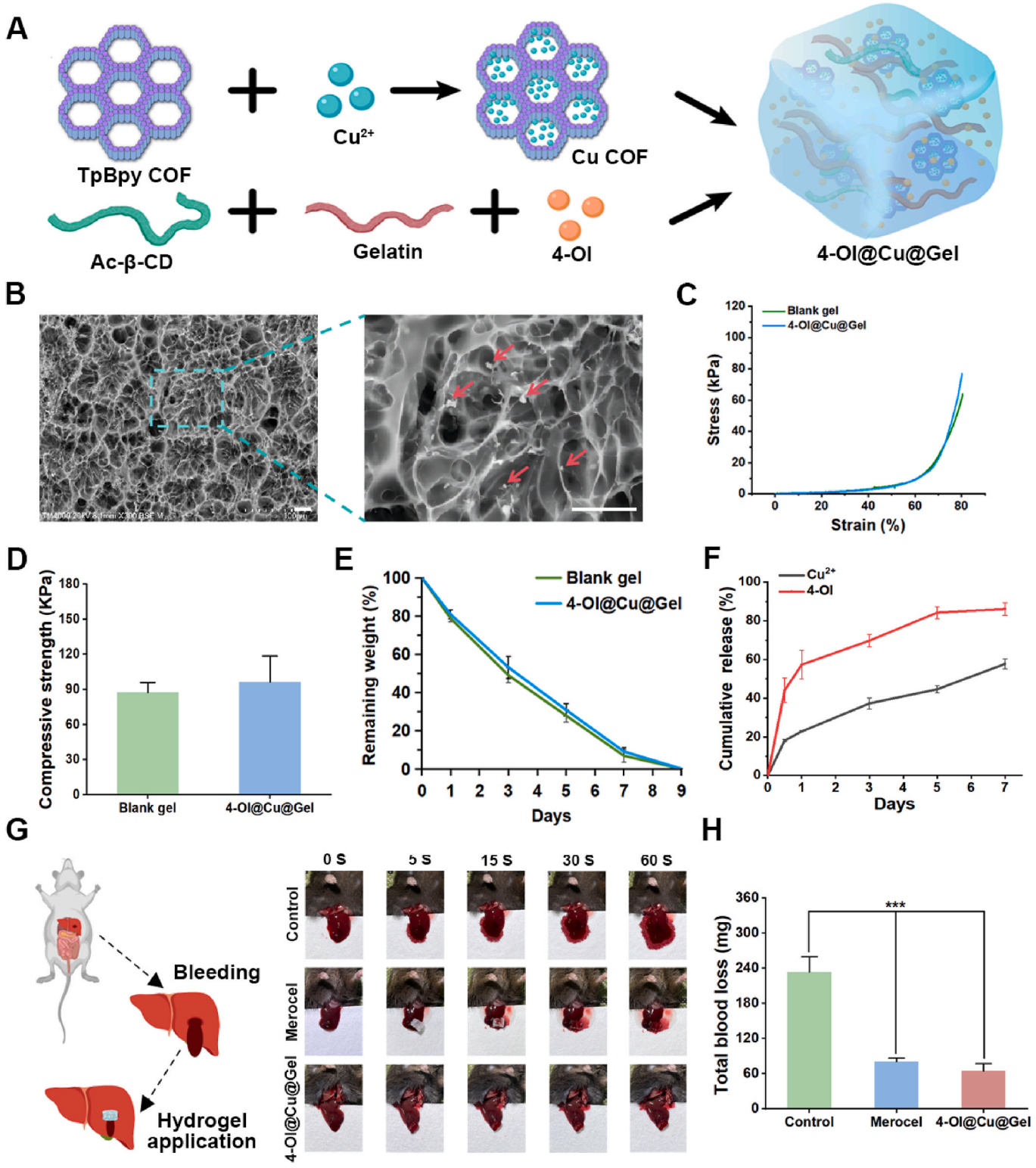

Fig. 2. Characterization of the 4-OI@Cu@Gel. (A) Schematic illustration of preparation of the 4-OI@Cu@Gel. (B) SEM images of the 4-OI@Cu@Gel. Scale bar = 25 μm. (C) Compression test of the blank gel and 4-OI@Cu@Gel. (D) Compressive strengths of the blank gel and 4-OI@Cu@Gel. (E) Degradation behavior of the blank gel and 4-OI@Cu@Gel. (F) The release test of 4-OI and Cu^{2+} in 4-OI@Cu@Gel. (G and H) Hemostatic property of the 4-OI@Cu@Gel. (*P < 0.05, **P < 0.01, ***P < 0.001).

2. Results

2.1. Characterization of Cu COF and 4-OI@Cu@Gel

The transmission electron microscope (TEM) images showed that the size of Cu COF was about 500 nm (Fig. S1). The results energy dispersive X-ray (EDX) analysis showed the distribution of Cu element in Cu COF (Fig. S2). Fig. S3 illustrated the network in gelatin/Ac-β-CD hydrogel. The hydrogel was chemically crosslinked among the acryloyl groups of Ac-β-CDs and was physically crosslinked through host–guest interactions between the acryloyl groups of Ac-β-CDs and aromatic residues of the gelatin. Fig. 2A and Fig. S4 showed the preparation process of 4-OI@Cu@Gel. 4-OI and Cu COF were directly added to the gelatin/Ac-β-CD solution in the process of fabricating hydrogels. The morphology of hydrogels was observed by scanning electron microscopy (SEM). As shown in Fig. 2B and Fig. S5, both blank gel and 4-OI@Cu@Gel had interconnected porous structures, and the pore size ranged from 20 to 60 μm. The red arrows indicated the Cu COF incorporated in 4-OI@Cu@Gel. The EDX analysis results in Fig. S6 further indicated the incorporation of Cu COF into the hydrogel. The rheological characteristics of the blank gel and 4-OI@Cu@Gel was similar (Fig. S7). The mechanical properties of the blank gel and 4-OI@Cu@Gel were also investigated. The results indicated that both the blank gel and 4-OI@Cu@Gel could sustain more than 80% compressive stress strain before rupture (Fig. 2C). The compressive strengths of the blank gel and 4-OI@Cu@Gel were 87.4 and 96.5 KPa, respectively (Fig. 2D). The blank gel and 4-OI@Cu@Gel were immersed in PBS at 37 °C to assess their degradation. As shown in Fig. 2E, the blank gel and 4-OI@Cu@Gel hydrogels exhibited similar degradation rates and were degraded completely on day 9. The results of release test of 4-OI and Cu^{2+} showed that the release of 4-OI was much faster than Cu^{2+}, especially in the first 5 days (Fig. 2F). The hemostatic ability of the hydrogels was investigated using a mouse liver hemorrhage model. Compared with that in the control group, the blood loss in the Merocel (a commercial hemostatic sponge) and 4-OI@Cu@Gel groups was significantly lower (Fig. 2G and H), indicating the excellent hemostatic function of the developed hydrogel.

2.2. 4-OI@Cu@Gel modulates macrophage polarization

To simulate the *in vivo* inflammatory environment, RAW264.7 cells were pre-stimulated with LPS. Subsequently, the cells were treated with different hydrogels or PBS to evaluate their effects on macrophage polarization. Flow cytometric analysis revealed that LPS-stimulated macrophages exhibited increased expression of CD86, a marker of M1 macrophages. Treatment with 4-OI@Cu@Gel reduced CD86 expression (Fig. 3A and C). LPS treatment did not significantly reduce the expression of CD206, a marker of M2 macrophages. Cu@Gel and 4-OI@Cu@Gel promoted the expression of CD206, with the highest CD206 expression occurring in the 4-OI@Cu@Gel group (Fig. 3B and D). This finding was confirmed by the results of immunofluorescence staining. Compared with those in the LPS and LPS + Cu@Gel groups, the macrophages in the LPS+4-OI@Cu@Gel group exhibited less CD86 immunostaining and more CD206 immunostaining (Fig. 3E–G). To explore the underlying mechanism, we conducted western blotting, and the results showed that 4-OI@Cu@Gel significantly induced the expression of Nrf2 (Fig. 3H), which is an important immunomodulator of macrophage polarization. The results in Fig. S8 further indicated that the Nrf2 was mainly expressed in the nucleus. Furthermore, the treatment with 4-OI@Cu@Gel significantly reduced the inflammatory cytokines secretion, including TNF-α and IL-1β (Fig. S9).

2.3. 4-OI@Cu@Gel promotes osteogenesis by enhancing glycolysis

The osteogenic differentiation of BMSCs is essential for bone regeneration and fracture healing. To investigate whether 4-OI@Cu@Gel could promote BMSC osteogenic differentiation by stimulating glycolysis, BMSCs at passage 3 was incubated with osteogenic induction medium supplemented with different hydrogels for 3 or 14 days. As shown in Fig. 4A, the expression of GLUT1 proteins was upregulated in BMSCs treated with Cu@Gel and 4-OI@Cu@Gel on day 3. This finding was consistent with the results of the qRT-PCR analysis (Fig. 4B). After treatment with Bay 87-2243, an inhibitor of HIF-1α, the promoting effect of 4-OI@Cu@Gel on HIF-1α and GLUT1 expression was abolished (Fig. S10). Additionally, we analyzed the mRNA levels of glycolysis-related genes after different treatments. Higher gene expression levels of *HK2*, *LDHA* and *PDK1* were detected in the Cu@Gel and 4-OI@Cu@Gel groups than for the control group (Fig. 4C). The lactate production of BMSCs was also enhanced by treatment with Cu@Gel and 4-OI@Cu@Gel (Fig. S11), indicating enhanced glycolysis induced by Cu^{2+}. For further evaluation, the gene expression of osteogenic markers, including *RUNX2* and *ALP*, was analyzed by qRT−PCR analysis. The results showed that the expression of these genes was elevated in the 4-OI@Cu@Gel group (Fig. 4D), suggesting enhanced osteogenic differentiation in this group. Subsequently, ALP and Alizarin red staining were conducted on day 14 to evaluate the osteogenic differentiation of the BMSCs. The staining depth of ALP in the Cu@Gel and 4-OI@Cu@Gel groups was greater than that in the control group, indicating that the ALP activity was greater in the BMSCs treated with Cu@Gel and 4-OI@Cu@Gel (Fig. 4E and F). Accordingly, Alizarin red staining showed that the Cu@Gel and 4-OI@Cu@Gel groups exhibited enhanced mineral deposition and calcium nodule formation (Fig. 4G and H). As shown in Fig. S12, treatment with 4-OI@Cu@Gel and Bay 87-2243 resulted in reduced ALP activity (Fig. S12). These results revealed that 4-OI@Cu@Gel can promote the osteogenic differentiation of BMSCs by stimulating glycolysis.

2.4. Angiogenic and antioxidative capacities of 4-OI@Cu@Gel

To assess the cytocompatibility of the hydrogels, we conducted live/dead staining and CCK-8 assay on HUEVCs. The results of live/dead staining revealed a continuous increase in the number of HUVECs treated with Cu@Gel and 4-OI@Cu@Gel, with no observable cell death, indicating low cytotoxicity of the hydrogels (Fig. 5A). Accordingly, the results of the CCK-8 assay showed that the proliferation rate of HUEVCs in the Cu@Gel and 4-OI@Cu@Gel groups was similar to that in the control group, as indicated by the similar OD values in each group (Fig. S13). Next, we evaluated the impact of the hydrogels on HUVEC angiogenesis by conducting scratch tests and tube formation assays. Notably, a faster wound closure rate was observed in the Cu@Gel and 4-OI@Cu@Gel groups than in the control group (Fig. 5B and C). Additionally, treatment with Cu@Gel or 4-OI@Cu@Gel significantly promoted the tube formation of HUVECs (Fig. 5D). The quantitative analysis indicated that the number of junctions and total branching length were greater in the Cu@Gel and 4-OI@Cu@Gel groups (Fig. 5E). Furthermore, we analyzed the expression of angiogenic genes, including *VEGF* and *CD31*, using qRT−PCR analysis. The results showed that the expression levels of *VEGF* and *CD31* in HUVECs treated with 4-OI@Cu@Gel were significantly increased (Fig. 5F). These findings indicated that the Cu@Gel and 4-OI@Cu@Gel were able to promote angiogenesis through the release of Cu^{2+}.

To investigate the antioxidative ability of 4-OI@Cu@Gel, we incubated HUEVCs with culture media supplemented with 500 μM H_2O_2 and PBS, Cu@Gel, or 4-OI@Cu@Gel. The addition of H_2O_2 resulted in obvious ROS accumulation in HUEVCs (Fig. S14). Notably, treatment with 4-OI@Cu@Gel significantly reduced the ROS level. In addition, we conducted cytoskeleton staining, and the results showed that cytoskeletal damage was occurred in HUEVCs treated with H_2O_2, while treatment with 4-OI@Cu@Gel alleviated this damage (Fig. S15), indicating that 4-OI@Cu@Gel protected cells from oxidative stress.

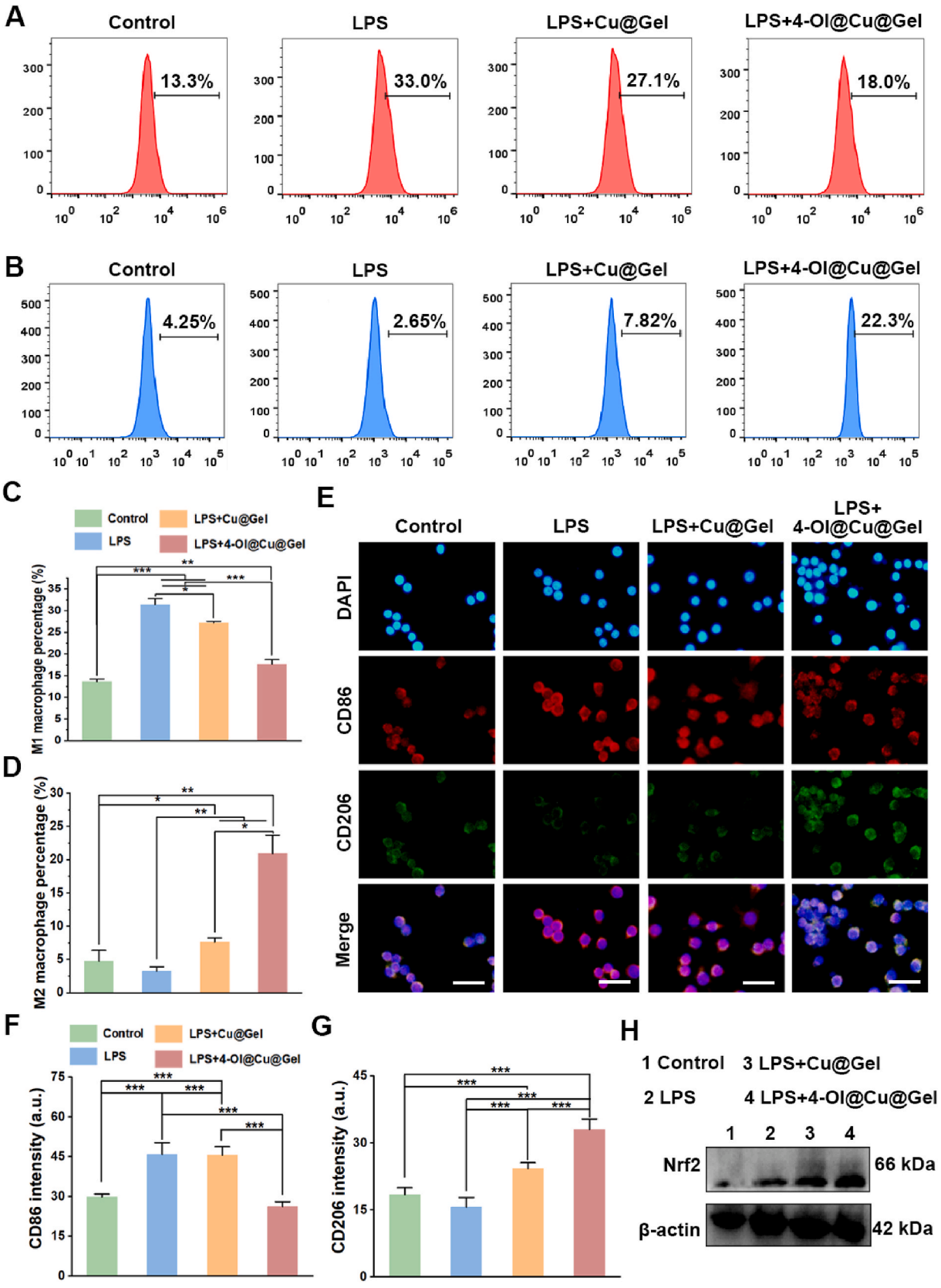

Fig. 3. The effects of 4-OI@Cu@Gel on macrophage polarization. (A and C) Flow cytometry analysis and corresponding quantitative analysis of CD86 expression in RAW264.7 cells. (B and D) Flow cytometry analysis and corresponding quantitative analysis of CD206 expression in RAW264.7 cells. (E–G) Immunofluorescence staining and corresponding quantitative analysis of CD86 and CD206 in RAW264.7 cells. Scale bar = 50 μm. (H) Western blot analysis of Nrf2 expression in RAW264.7 cells after different treatments. (*P < 0.05, **P < 0.01, ***P < 0.001).

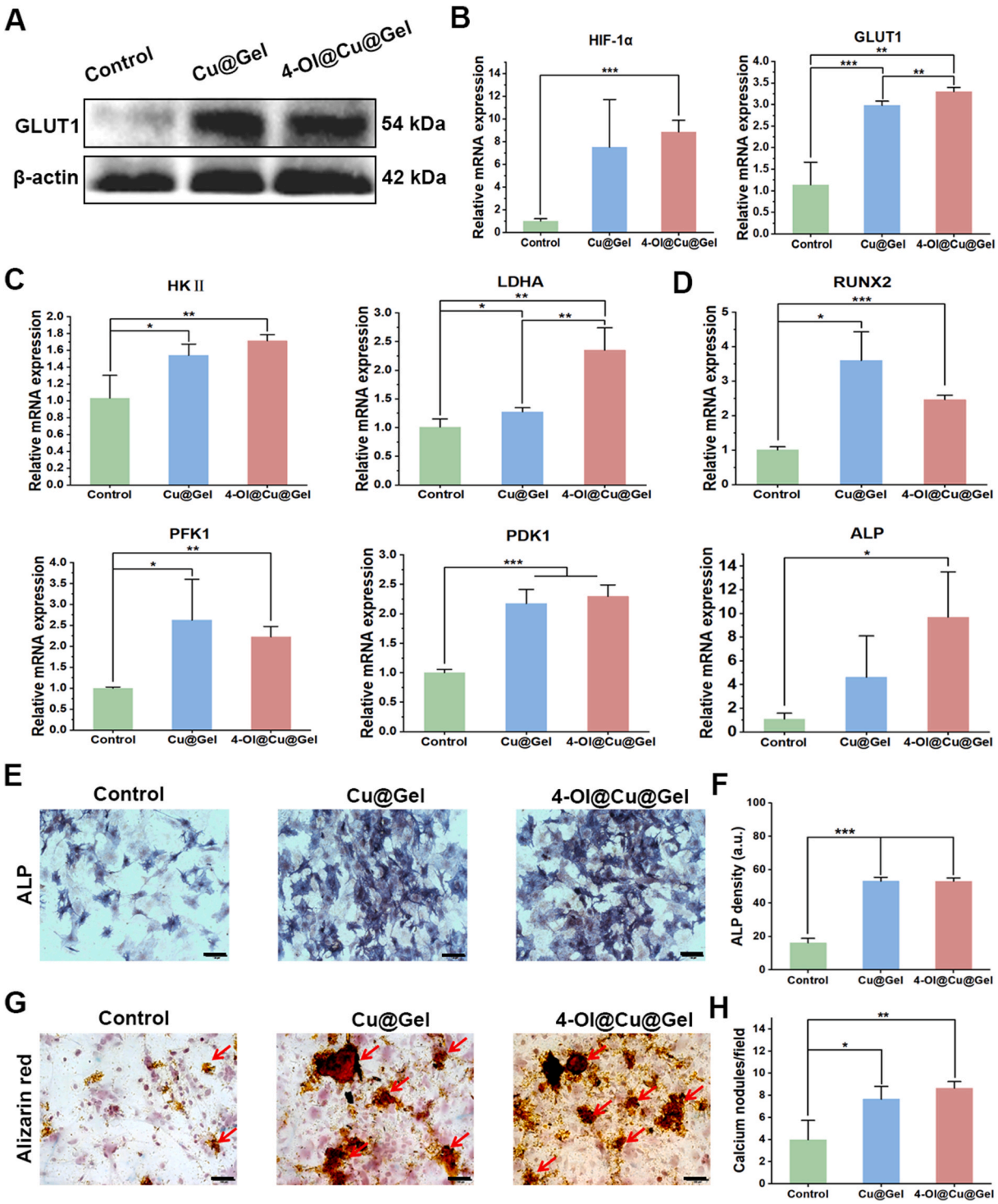

Fig. 4. 4-OI@Cu@Gel stimulated glycolysis and promoted osteogenic the differentiation of BMSCs. (A) Western blot analysis of GLUT1 expressions in BMSCs after different treatments. (B) qRT−PCR analysis of *HIF-1α* and *GLUT1* expression in BMSCs after different treatments (48 h). (C) qRT−PCR analysis of glycolysis-related genes, including *HK2*, *LDHA*, *PFK1* and *PDK1*, in BMSCs after different treatments. (D) qRT−PCR analysis of osteogenic genes, including *RUNX2* and *ALP*, in BMSCs after different treatments. (E and F) ALP staining results of BMSCs after osteogenic differentiation induction (14 days) and different treatments. Scale bar = 100 μm. (G and H) Alizarin red staining results of BMSCs after osteogenic differentiation induction (14 days) and different treatments. Scale bar = 50 μm. (*P < 0.05, **P < 0.01, ***P < 0.001).

2.5. *In vivo fracture healing with 4-OI@Cu@Gel*

To investigate whether 4-OI@Cu@Gel could promote fracture healing and tissue regeneration *in vivo*, we assessed bone fracture healing in a femoral fracture mouse model. The fracture sites were treated with Cu@Gel, 4-OI@Cu@Gel, or PBS as a control. X-ray, microcomputed tomography (micro-CT) and histologic analyses were conducted to monitor fracture healing after surgery (Fig. 6A). The results of X ray examination showed that a fracture gap could be observed in all the groups 7 days after surgery. On day 21, the Cu@Gel and 4-OI@Cu@Gel groups exhibited a fuzzy fracture line, while the control group still showed a visible fracture line (Fig. 6B). As shown in Fig. 6C

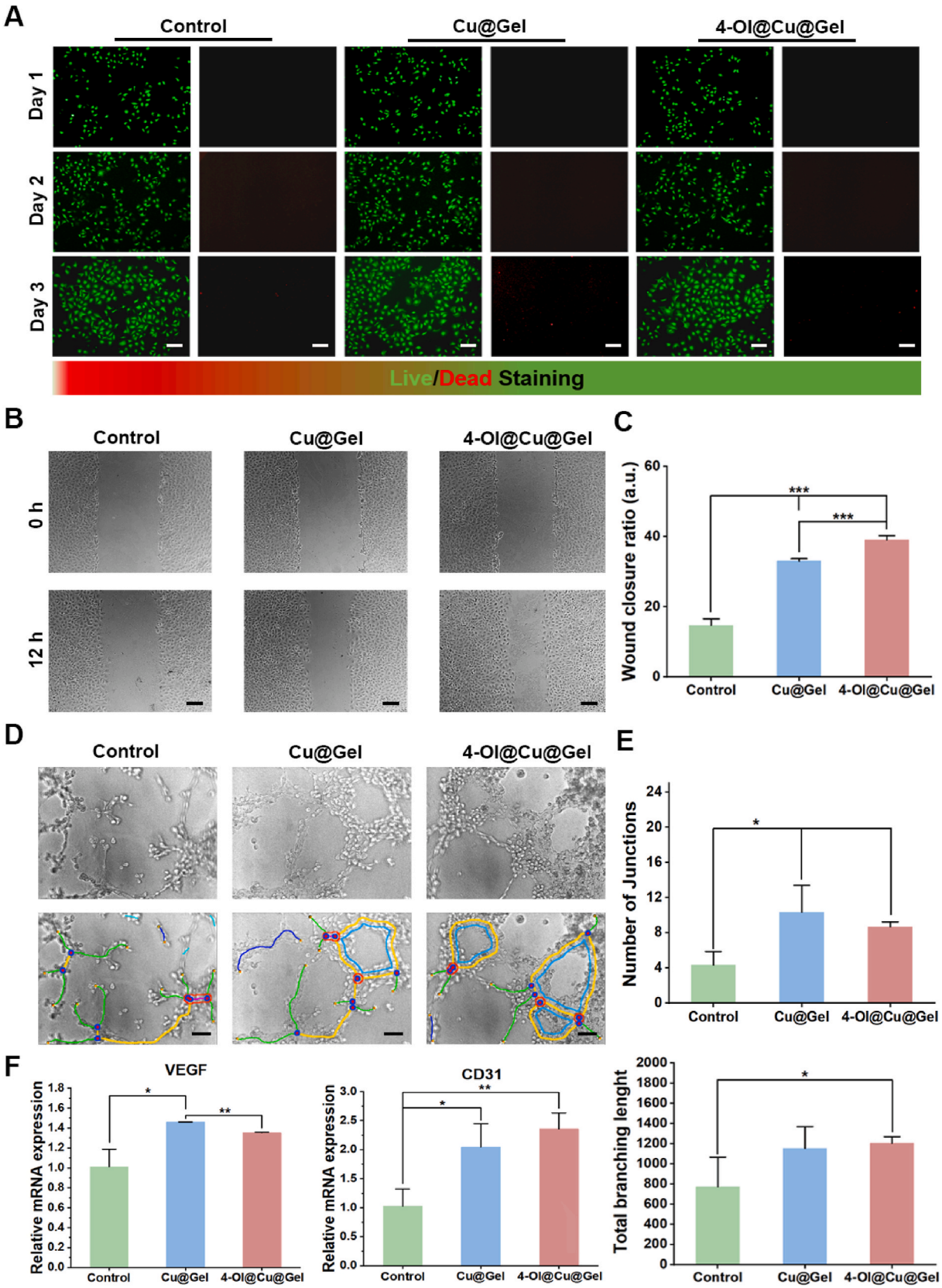

Fig. 5. Angiogenic properties of 4-OI@Cu@Gel. (A) Live/dead staining of HUEVCs treated with PBS, Cu@Gel or 4-OI@Cu@Gel. Scale bar = 100 μm. (B and C) Scratch assay and corresponding quantitative analysis. Scale bar = 100 μm. (D and E) Tube formation assay and corresponding quantitative analysis. Scale bar = 50 μm. (F) qRT−PCR analysis of *VEGF* and *CD31* in HUVECs after different treatments. (*P < 0.05, **P < 0.01, ***P < 0.001).

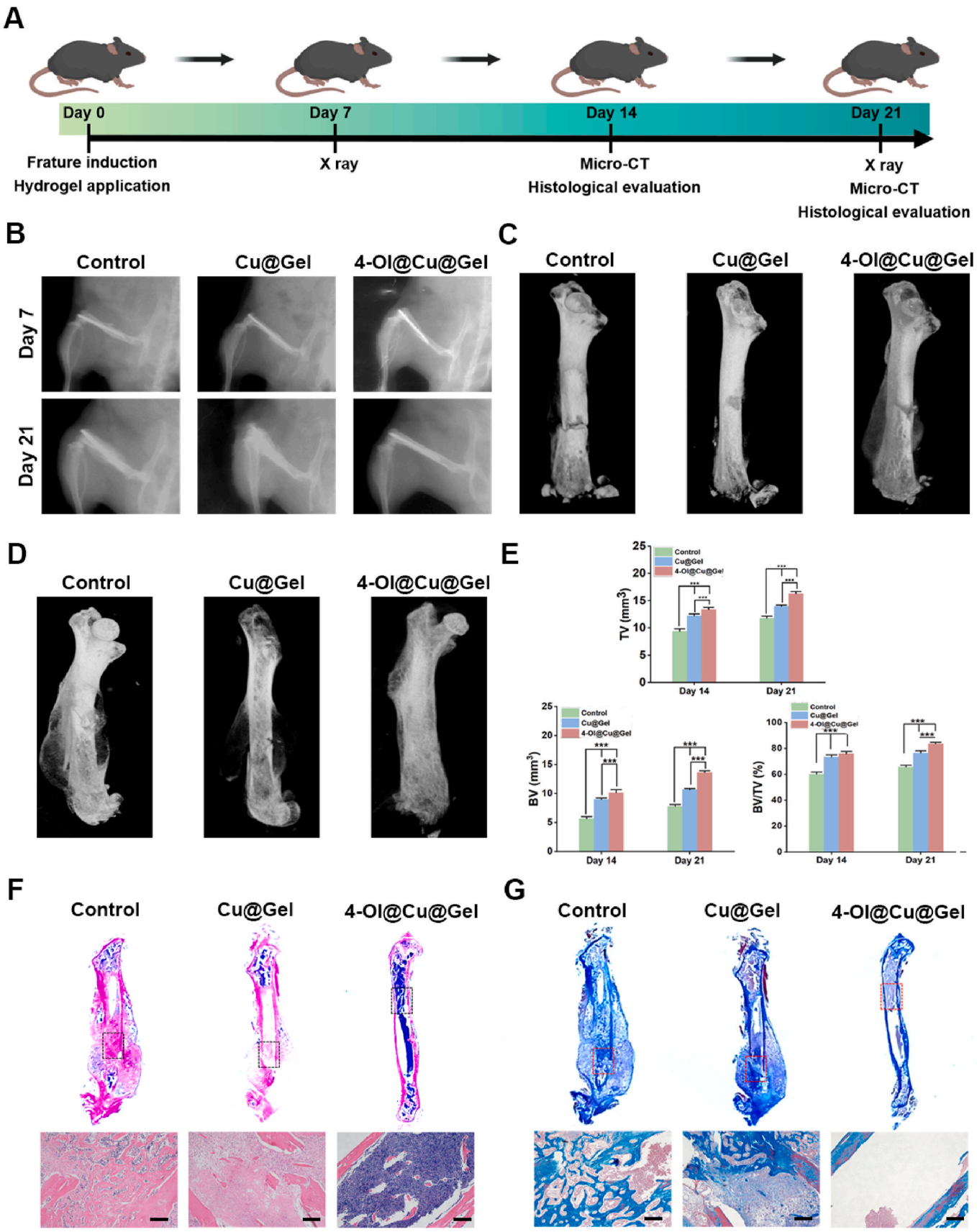

Fig. 6. 4-OI@Cu@Gel accelerated fracture healing in mice. (A) The timeline of the *in vivo* experiment. (B) X-ray images of the femurs on days 7 and 21. Micro-CT construction images on days 14 (C) and 21 (D). (E) Statistical analysis of the micro-CT results, including TV, BV and BV/TV. (F) H&E staining of femurs harvested on day 21. Scale bar = 100 μm. (G) Masson's trichrome staining of the femurs collected on day 21. Scale bar = 100 μm. (*P < 0.05, **P < 0.01, ***P < 0.001).

and D, the formation of bony callus was observed in all the groups, with the greatest amount of bone formation occurring in the 4-OI@Cu@Gel group on days 14 and 21. The 4-OI@Cu@Gel group had the highest tissue volume (TV), bone volume (BV) and BV/TV among the groups, while the control group had the lowest (Fig. 6E). Accordingly, the results of hematoxylin and eosin (H&E) staining demonstrated denser bone formation and better bone continuity in the 4-OI@Cu@Gel group than in the other groups (Fig. 6F). The results of Masson's trichrome staining also revealed more pronounced new bone formation and mature bone tissue in the fracture callus in the 4-OI@Cu@Gel group (Fig. 6G). These results indicated that 4-OI@Cu@Gel could effectively promote fracture healing *in vivo*.

2.6. Histological analysis

Immunohistochemical (IHC) staining indicated increased expressions of Nrf2 (Fig. 7A and B) in the 4-OI@Cu@Gel group on day 14. The macrophage polarization was determined by immunofluorescence staining for CD86 and CD206. The results showed that $CD86^+$ cells were decreased (Fig. 7C and D), while $CD206^+$ cells were increased (Fig. 7E and F), in the 4-OI@Cu@Gel group at day 14, indicating 4-OI@Cu@Gel inhibited M1 macrophage polarization and promoted M2 macrophage polarization *in vivo*. The results of IHC staining for IL-1β further indicated that 4-OI@Cu@Gel reduced inflammatory response (Fig. 7G and H). Dihydroethidium (DHE) staining was conducted to evaluate the ROS levels in the fracture sites. Notably, a significantly reduced ROS level (red stained area) was observed in the 4-OI@Cu@Gel group compared with the other groups (Fig. S16), suggesting that oxidative stress was alleviated at the fracture site. The results of IHC staining for PDK1 showed that Cu@Gel and 4-OI@Cu@Gel increased PDK1 expression *in vivo* (Fig. S17). Furthermore, IHC staining indicated robust expression of OCN (Fig. 8A and B) and RUNX2 (Fig. 8C and D) in the 4-OI@Cu@Gel group on day 21, which was in agreement with the Masson trichrome staining results. To assess vessel formation, IHC staining for VEGF and CD31 was performed. VEGF (Fig. 8E and F) and CD31 (Fig. 8G and H) expression was significantly increased in the Cu@Gel and 4-OI@Cu@Gel groups, indicating that both the Cu@Gel and 4-OI@Cu@Gel enhanced vascularization during fracture healing. In summary, 4-OI@Cu@Gel promoted tissue regeneration and accelerated bone maturation *in vivo*.

3. Discussion

Fracture healing is a dynamic process that can be categorized into three phases: the inflammatory phase, the repair phase, and the remodeling phase [28]. The development of composite hydrogels for sequence release of different drugs represents an efficient approach to guide bone healing [29]. The optimal transient stage of acute inflammation and functional tissue regeneration are crucial for successful fracture healing. During the whole course of fracture healing, macrophages and BMSCs participate in phase transformation to regulate healing [30,31]. Thus, finding approaches to spontaneously modulate the metabolism and function of macrophages and BMSCs is key to regulating the metabolic microenvironment for improved bone healing. It has been demonstrated that Nrf2 is involved in the regulation of redox, carbohydrate and lipid metabolism in macrophages following LPS treatment. Nrf2 activation facilitates metabolic reprogramming and mitochondrial fusion, leading to a suppressed inflammatory response [32]. Zhang et al. indicated that expression of lysine acetyltransferase 2A (KAT2A) in macrophages suppressed Nrf2 activity, resulting in an increased inflammatory response and bone destruction in rheumatoid arthritis [33]. The metabolism of BMSCs can also be remodeled to finetune their functions. For example, Liu et al. reported that overexpression (OE) of nucleosome assembly protein 1-like 2 (Nap1l2) induced impaired immunomodulation in BMSCs, accompanied by changes in glycolysis/gluconeogenesis, fatty acid metabolism, and amino acid metabolism. Treatment with metformin was able to rescue the immunomodulation property of the OE-Nap1l2 BMSCs by suppressing oxidative phosphorylation and increasing the AMP/ATP ratio [34]. In this study, we fabricated a nanocomposite hydrogel for the delivery of 4-OI and Cu^{2+} and regulation of metabolic microenvironment at the fracture site. The results showed that the burst release of 4-OI reduced M1 macrophage polarization and oxidative stress, while the sustained release of Cu^{2+} enhanced bone regeneration and vascularization, resulting in robust bone healing *in vivo*.

During the past decade, Cu-doped biomaterials have shown great potential in bone healing due to their excellent antibacterial and angiogenic properties [35]. Recently, the effect of Cu-doped biomaterials on osteogenesis has also been verified [36–38], but the underlying molecular mechanism has not been determined. In this study, we confirmed that Cu^{2+} enhanced BMSC osteogenic differentiation by promoting glycolysis through activation of the HIF-1α-GLUT1 signaling pathway. To our knowledge, this is the first study in which the underlying mechanism by which Cu-doped biomaterials stimulate cellular glycolysis and osteogenesis has been demonstrated. Furthermore, we found that the macrophages in the Cu@Gel group exhibited increased Nrf2 expression compared with those in the control group, indicating that Cu^{2+} could induce activation of Nrf2, which is consistent with the findings of previous studies [39,40]. However, the application of Cu-doped biomaterials is limited by the potential toxicity of Cu^{2+} since an overdose of Cu^{2+} can induce cuproptosis and oxidative damage [41]. Reducing the toxicity of Cu^{2+} is key to promoting the clinical application of Cu-doped biomaterials for tissue repair. In this study, we incorporated Cu^{2+} into COFs to allow for sustained and slow Cu^{2+} release. Furthermore, the 4-OI in the composite hydrogel could activate Nrf2 and alleviate oxidative stress in normal cells, thus reducing the toxicity of Cu^{2+} to a certain extent.

4-OI is a synthetic permeable itaconate derivative that has excellent antioxidant and anti-inflammatory effects. 4-OI alleviates tissue injury and regulates immune balance via activation of the Nrf2 signaling pathway [42,43]. For example, Xiao et al. loaded 4-OI into an oxidized sodium alginate/gelatin hydrogel to treat cartilage damage and confirmed that the developed hydrogel was able to promote M2 macrophage polarization and inhibit inflammatory responses, thus promoting cartilage regeneration [44]. However, little has been reported about the application of 4-OI for the treatment of fractures and bone defects. In this study, the burst release of 4-OI was able to reduce the inflammatory response in the early stage of fracture healing. Interestingly, we found that the BMSCs in the 4-OI@Cu@Gel group expressed higher levels of *LDHA* than that in the Cu@Gel group. The AMPK signaling pathway is also involved in the modulation of glycolysis. It has been demonstrated that itaconate can regulate AMPK phosphorylation [45–47]. 4-OI may also impact BMSC glycolysis through regulation of the MAPK signaling pathway. Further investigation is needed in the future.

There are several limitations to our study. First, immediately upon tissue damage, an immune cell- and molecular factor-engaged inflammatory response is triggered, ultimately initiating the repair cascade. The initiation of fracture healing after injury relies heavily on the acute inflammatory response. Hindered fracture healing can occur when natural acute inflammation processes are impeded or when chronic inflammation arises due to an ongoing adverse stimulus [5]. The precise regulation of inflammation to initiate endogenous fracture healing and avoid chronic inflammation should be further explored. Second, our study investigated the metabolic reprogramming of macrophages and BMSCs to improve bone fracture healing. The 4-OI@Cu@Gel nanocomposite hydrogel was applied at the fracture site, and it remains unknown whether 4-OI@Cu@Gel affects other cells, such as neutrophils, T cells, and osteoclasts. In the future, we will develop a targeted drug delivery system to accurately modulate the functions of macrophages and BMSCs. In addition, the effects of the physical properties of hydrogels on cell responses need to be further determined by directly

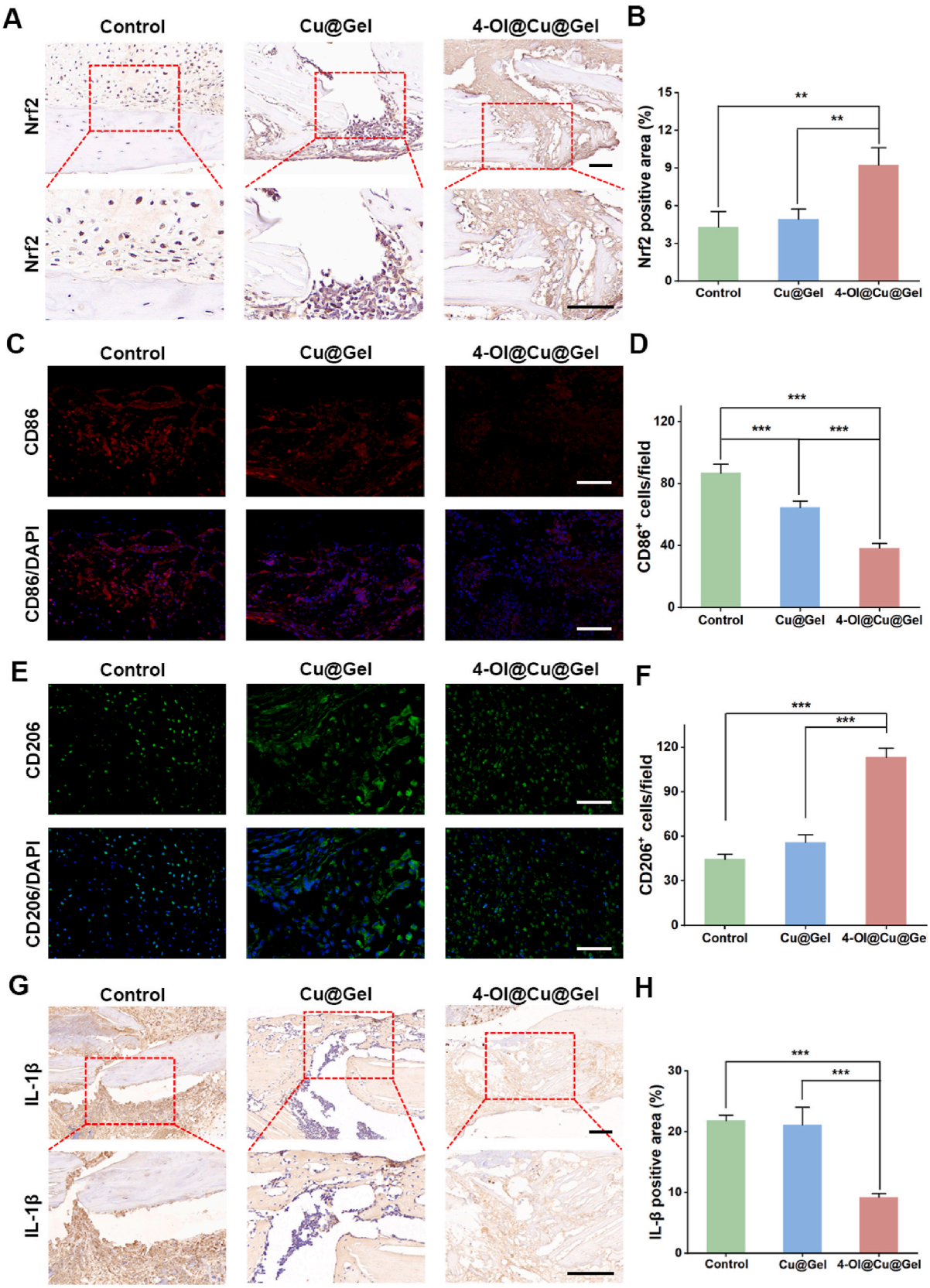

Fig. 7. 4-OI@Cu@Gel modulated the inflammatory response *in vivo*. (A and B) IHC staining for Nrf2 expression and corresponding quantitative analysis on day 14. Scale bar = 50 μm. (C and D) CD86 immunofluorescence staining of bone tissue and corresponding quantitative analysis on day 14. Scale bar = 50 μm. (E and F) CD206 immunofluorescence staining of bone tissue and corresponding quantitative analysis on day 14. Scale bar = 50 μm. (G and H) IHC staining for IL-1β expression and corresponding quantitative analysis on day 14. Scale bar = 100 μm. (*P < 0.05, **P < 0.01, ***P < 0.001).

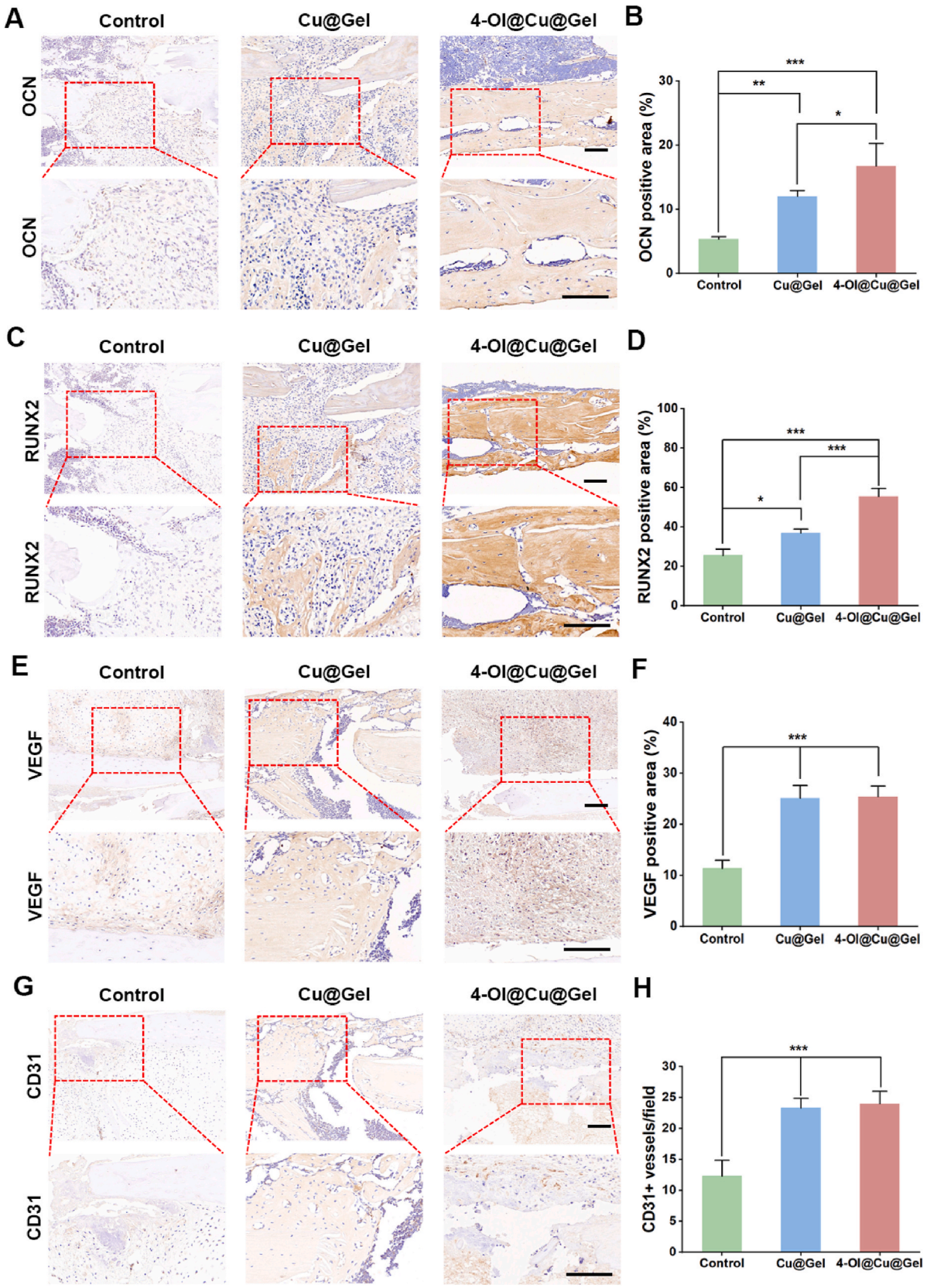

Fig. 8. 4-OI@Cu@Gel promoted bone regeneration and vessel formation *in vivo*. (A and B) IHC staining for OCN expression and corresponding quantitative analysis on day 21. Scale bar = 100 μm. (C and D) IHC staining for RUNX2 expression and corresponding quantitative analysis on day 21. Scale bar = 100 μm. (E and F) IHC staining for VEGF expression and corresponding quantitative analysis on day 14. Scale bar = 100 μm. (G and H) IHC staining for CD31 expression and corresponding quantitative analysis on day 14. Scale bar = 100 μm. (*P < 0.05, **P < 0.01, ***P < 0.001).

seeding the cells onto the hydrogels. Third, in this study, our core objective is to confirm that the therapeutic effect of 4-OI@Cu@Gel is better than Cu@Gel and blank (PBS). However, the groups of blank (PBS), Gel, 4-OI@Gel, Cu@Gel, and 4-OI@Cu@Gel, are more reasonable. In our future works, we will conduct more comprehensive comparison to improve the systematic ness and integrity. Fourth, week 3 was selected as the primary endpoint according to our established protocol. Despite the lack of cytotoxicity and accelerated fracture healing in the 4-OI@Cu@Gel group, a longer observation time may be needed to evaluate the long-term outcome and adverse effect of the treatment.

4. Conclusion

In summary, we developed a nanocomposite hydrogel to improve bone fracture healing. The 4-OI@Cu@Gel hydrogel, which acted as a metabolic regulator during fracture healing, can deliver 4-OI to reduce the inflammatory response, promote M2 macrophage polarization and alleviate oxidative stress at the early stage and Cu^{2+} to stimulate BMSC glycolysis and osteogenic differentiation and endothelial cell angiogenesis at the later stage. Concurrently, the hydrogel reduced the inflammatory response, alleviated oxidative damage, enhanced vascularization and bone formation, and promoted fracture healing *in vivo*. Therefore, these findings could lead to the use of a novel therapeutic strategy for the treatment of fractures and bone defects.

5. Experimental section

5.1. Fabrication of the Cu COF

First, TpBpy-COF was synthesized according to a reported method [48]. In brief, 2,4,6-triformylphloroglucinol (Tp) (0.4 mmoL, 84.0 mg) and 2,2′-dipyridine-5,5′-diamine (Bpy) (0.6 mmoL, 111.6 mg) were added to a Schlenk tube containing mesitylene (2 mL), 1,4-dioxane (2 mL), and 6 M aqueous acetic acid (0.4 mL). The tube was then subjected to degassing for freeze–pump–thaw cycles at 77 K (using a liquid nitrogen bath), followed by evacuation and sealing. Upon reaching room temperature, the tube was heated at 120 °C for 3 days. Afterwards, the product was collected, washed with anhydrous THF, subjected to Soxhlet extraction, and eventually dried under vacuum at 60 °C for 24 h to yield TpBpy-COF. To fabricate Cu-TpBpy-COF, TpBpy-COF (65 mg) and copper acetate (35 mg) were dispersed in ethanol (45 mL) via ultrasonic treatment. The resulting solution was continuously stirred for 6 h at 45 °C. The resulting solid was collected via centrifugation and washed with methanol. Finally, the powder was dried under vacuum at 80 °C for 24 h to obtain Cu-TpBpy-COF (Cu COF).

5.2. Synthesis of Ac-β-CD

β-Cyclodextrin (10 g) was dissolved in a mixed solution of dimethyl formamide (150 mL) and triethylamine (7 mL). Then, acrylic acid (7 mL) was added to the mixture, which was stirred on ice for 12 h. Afterwards, the mixture was filtered and concentrated via vacuum rotary evaporation. The product was then washed with acetone and dried under vacuum for 72 h to obtain Ac-β-CD.

5.3. Preparation of 4-OI@Cu@Gel

Gelatin (1 g) and Ac-β-CD (1 g) were dissolved in PBS (12 mL) at 37 °C. After that, 4-OI (50 mg) and Cu COF (5 mg) were added to the mixture. The solution was then mixed with Irgacure and irradiated with ultraviolet for 15 min to form 4-OI@Cu@Gel.

5.4. Characterization of the 4-OI@Cu@Gel

The morphology of the Cu COF and hydrogels was observed via TEM and SEM (LIBRA 200 CS, Carl Zeiss Co., Germany).

The compressive mechanical characteristics of the blank gel and 4-OI@Cu@Gel (3 mm thick) were detected using a MACH-1 Micromechanical System (Biomomentum, Inc., Canada). The compressive strength was calculated by using the following equation: $F = P/A$, where F refers to the compressive strength, P refers to the maximum load, A refers to the cross-section of the area.

For the degradation test, the blank gel and 4-OI@Cu@Gel were weighed and incubated in PBS at 37 °C. At predetermined time intervals, the hydrogels were removed from PBS, dried at 37 °C, and weighed.

For the drug release test, the 4-OI@Cu@Gel was incubated in PBS at 37 °C. The supernatant was collected at different time points. The amount of 4-OI was determined by multimode plate reader. The amount of Cu^{2+} was measured by a Cu^{2+} detection kit (Leagene Biotechnology, Beijing, China) following the manufacturer's instructions.

For rheological test, time sweep was performed on a rheometer (MCR301, Anton Paar Co., Austria).

5.5. Hemostasis test

To evaluate the hemostatic ability of the hydrogels, a mouse model of liver hemorrhage was established. Briefly, the mice were first anesthetized, after which a surgical incision was made to expose the liver. To ensure accurate measurement of blood weight, the fluid around the lesion was carefully removed. Then, a predetermined weight filter paper (W0) was placed below the liver, and bleeding was produced by making a puncture in the liver using an 18 G needle. Subsequently, the hydrogels were immediately inserted into the wound site. The liver wounds were photographed at 0, 5, 15, 30, and 60 s. Finally, the filter paper with accumulated blood was weighed (W1). The amount of blood loss was calculated as the difference in weight (W1–W0) of the filter paper.

5.6. Flow cytometry assay

First, RAW 264.7 cells were seeded into 6-well plates at a density of 2×10^5 cells per well and incubated with culture medium containing 250 ng/mL LPS and different hydrogel extractions or PBS. After 12 h of incubation, the cells were obtained and stained with an anti-CD86 antibody and an anti-CD206 antibody according to the manufacturer's instructions. The cells were then collected by centrifugation, washed with PBS and measured by flow cytometry. The results were analyzed with FlowJo_V10 software.

5.7. Immunofluorescence staining

After different treatments, the cells were washed with PBS, fixed with 4% paraformaldehyde, permeabilized with 0.1% Triton X-100, and blocked with 10% goat serum. Subsequently, the cells were stained with an anti-CD86 antibody and anti-CD206 antibody at 4 °C overnight. The cells were then washed and incubated with secondary antibodies, followed by DAPI staining and observation for further analysis.

5.8. In vitro osteogenic differentiation

BMSCs were extracted from mouse femurs and cultured in DMEM supplemented with 10% FBS. At passage 3, BMSCs were seeded into 24-well plates at a density of 1×10^5 cells per well. Then, osteogenic differentiation was induced by the addition of 10 mM β-glycerophosphate, 10 nM dexamethasone, and 50 μg/ml ascorbic acid. Moreover, the cells received different treatments. The culture medium was changed every 3 days. After 14 days, ALP and Alizarin red S staining were performed to evaluate the osteogenic differentiation of the different groups.

5.9. qRT–PCR analysis

Total RNA was extracted from cultured cells using TRIzol reagent. The RNA was reverse transcribed with a reverse transcription kit. Quantitative

real-time PCR was performed using AceQqPCR SYBR Green Master Mix according to the manufacturer's instructions. All primers were synthesized by Sangon Biotech. The primers used were as follows: ALP-forward: CCAACTCTTTTGTGCCAGAGA, ALP-reverse: GCTACATTGGTGTTGAGC TTTT; RUNX2-forward: CGCCACCACTCACTACCACAC; RUNX2-reverse: TGGATTTAATAGCGTGCTGCC; HIF-1α-forward: ACCTTCATCGGAAA CTCCAAAG; HIF-1α-reverse: CTGTTAGGCTGGGAAAAGTTAGG; GLUT1-forward: ACCGTGACGGAATCCTTCTCT; GLUT1-reverse: GCCCCCGA-CAGAGAAGATG; HK2-forward: TGATCGCCTGCTTATTCACGG; HK2-reverse: AACCGCCTAGAAATCTCCAGA; LDHA-forward: TGTCTCCAG-CAAAGACTACTGT; LDHA-reverse: GACTGTACTTGACAATGTTGGGA; PFK1-forward: TGTGGTCCGAGTTGGTATCTT; PFK1-reverse: GCACTTC-CAATCACTGTGCC; PDK1-forward: GGACTTCGGGTCAGTGAATGC; PDK1-reverse: TCCTGAGAAGATTGTCGGGGA; VEGF-forward: AGGGCA GAATCATCACGAAGT; VEGF-reverse: AGGGTCTCGATTGGATGGCA; CD31-forward: ACCGTGACGGAATCCTTCTCT; CD31-reverse: GCTGGAC TCCACTTTGCAC; mouse β-actin-forward: GGCTGTATTCCCCTCCATCG; mouse β-action-reverse: CCAGTTGGTAACAATGCCATGT; human β-actin-forward: CATGTACGTTGCTATCCAGGC; and human β-action-reverse: CTCCTTAATGTCACGCACGAT.

5.10. Western blots

The protein concentration was determined using the BCA Protein Assay Kit (Beyotime). Next, 30 μg of sample was loaded on a 10% SDS–polyacrylamide gel and separated via electrophoresis. Subsequently, the samples were transferred to nitrocellulose membranes and blocked with skim milk at room temperature for 1 h. Then, the samples were incubated with the corresponding primary antibodies overnight. The membranes were then washed with TBST, incubated with secondary antibodies for 1 h at room temperature, and visualized with a ChemiDoc MP chemiluminescence gel imaging system.

5.11. Cytocompatibility test

HUVECs were seeded into 96-well plates and treated with either PBS or different hydrogels. After culturing for 24 h, 48 h and 72 h, a CCK-8 assay was conducted to evaluate cell proliferation. The absorbance was measured by a microplate reader at 450 nm. Subsequently, calcein-AM/PI staining was used to evaluate cell viability. Images were acquired using a fluorescence microscope.

5.12. Scratch assay

HUEVCs were seeded in 6-well plates at a density of 3×10^5 cells per well. When the cells reached 90% confluence, a 200 μL pipette tip was used to make a scratch. The cells were washed three times with PBS and cultured with fetal bovine serum (FBS)-free DMEM containing different hydrogels. Subsequently, the cells were observed and photographed at 0 and 12 h using a microscope. The wound area was analyzed using ImageJ software.

5.13. Tube formation assay

Tube formation experiments were conducted to further investigate the effect of 4-OI@Cu@Gel on angiogenesis in HUEVCs. Briefly, HUEVCs were pretreated with different hydrogels overnight and then seeded in 96-well plates pretreated with Matrigel at a density of 2×10^4 cells per well. The cells were incubated for 6 h at 37 °C under 5% CO_2. Then, the cells were observed and photographed using light microscopy. The number of junctions and total branching length were analyzed by ImageJ software.

5.14. ROS scavenging test

HUVECs were seeded into 96-well plates at a density of 1×10^4 cells per well and incubated with 500 μM H_2O_2 and hydrogels or PBS for 12 h. Afterwards, the HUVECs were stained with the DCFH-DA probe at room temperature in the dark for 30 min to determine the cellular ROS level. For cytoskeleton staining, HUVECs were fixed with 4% paraformaldehyde, washed with PBS, and stained with phalloidin at room temperature in the dark for 30 min, followed by DAPI staining for 10 min. Images were obtained using fluorescence microscopy.

5.15. Murine femur fracture model

To assess the therapeutic effect of 4-OI@Cu@Gel on fractures, a murine femur fracture model was established. Briefly, male C57BL/6 mice (6 weeks old) were anesthetized with sodium pentobarbital. Then, the right hind leg was shaved and disinfected with iodine. A lateral skin incision was made in the right thigh, and the femur shaft was exposed by blunt dissection. Next, a needle was inserted parallel to the marrow cavity, and a diaphysis fracture was made in the middle of the femur using ophthalmic scissors. Then, 5 μL PBS, Cu@Gel, or 4-OI@Cu@Gel hydrogel was administered around the fracture sites ($n = 6$). During tissue dissection, we attempted to minimize tissue damage as much as possible. The adjacent fascia and muscle were sutured well to fix the hydrogel. Finally, the skin was sutured, and the surgical area was disinfected.

5.16. X-ray examination

On days 7 and 21 post fracture, X-ray examination was conducted with an In-Vivo FX PRO imaging system (Bruker, Karlsruhe, Germany) to monitor the fracture healing process.

5.17. Micro-CT scanning

The femur samples were harvested on days 14 and 21 and subjected to micro-CT scanning (Brucker micro-CT, Belgium). Image reconstruction was performed using CT-Vox version 2.1 software. CTAN version 1.12 software was used to measure the scanned images, and parameters such as TV, BV, and BV/TV were obtained.

5.18. Histological staining

The collected femurs were fixed in 4% paraformaldehyde for 48 h and washed three times. The samples were subsequently decalcified in 10% ethylenediaminetetraacetic acid (EDTA) for 3 weeks. Subsequently, the samples were embedded in paraffin and sliced into 6 μm sections. H&E, Masson, DHE and IHC staining were performed to evaluate the new bone tissues. Images of the sections were obtained using a microscope (Olympus).

5.19. Statistical analysis

The data are expressed as the mean ± standard deviation (SD) and were analyzed using Student's *t*-test and one-way ANOVA. SPSS 26.0 software was used for statistical analysis. A value of $p < 0.05$ indicated statistical significance.

Ethics approval

The procedures involving the use of animals were approved by the animal research ethics committee of Tongji Medical College, Huazhong University of Science and Technology.

CRediT authorship contribution statement

Kangkang Zha: Writing – review & editing, Writing – original draft, Methodology, Conceptualization. **Meijun Tan:** Writing – original draft, Methodology, Formal analysis. **Yiqiang Hu:** Writing – review & editing,

Writing – original draft, Conceptualization. **Weixian Hu:** Writing – review & editing, Methodology, Investigation. **Shengming Zhang:** Methodology. **Yanzhi Zhao:** Visualization. **Ze Lin:** Software, Resources. **Wenqian Zhang:** Formal analysis. **Hang Xue:** Resources, Funding acquisition. **Bobin Mi:** Writing – review & editing. **Wu Zhou:** Supervision, Conceptualization. **Qian Feng:** Validation, Supervision, Conceptualization. **Faqi Cao:** Supervision, Data curation, Conceptualization. **Guohui Liu:** Supervision, Project administration, Funding acquisition, Data curation, Conceptualization.

Declaration of competing interest

The authors declare that they have no known competing financial interests or personal relationships that could appear to influence the work reported in this paper.

Acknowledgments

This work was supported by the National Natural Science Foundation of China (No. 82272491, 82072444, 82202676).

Appendix A. Supplementary data

Supplementary data to this article can be found online at https://doi.org/10.1016/j.bioactmat.2024.03.025.

References

[1] C.W. Sing, T.C. Lin, S. Bartholomew, J.S. Bell, C. Bennett, K. Beyene, P. Bosco-Levy, B.D. Bradbury, A.H.Y. Chan, M. Chandran, C. Cooper, M. de Ridder, C.Y. Doyon, C. Droz-Perroteau, G. Ganesan, S. Hartikainen, J. Ilomaki, H.E. Jeong, D.P. Kiel, K. Kubota, E.C. Lai, J.L. Lange, E.M. Lewiecki, J. Lin, J. Liu, J. Maskell, M.M. de Abreu, J. O'Kelly, N. Ooba, A.B. Pedersen, A. Prats-Uribe, D. Prieto-Alhambra, S. X. Qin, J.Y. Shin, H.T. Sorensen, K.B. Tan, T. Thomas, A.M. Tolppanen, K.M. C. Verhamme, G.H. Wang, S. Watcharathanakij, S.J. Wood, C.L. Cheung, I.C. K. Wong, Global epidemiology of hip fractures: secular trends in incidence rate, post-fracture treatment, and all-cause mortality, J. Bone Miner. Res. 38 (8) (2023) 1064–1075.

[2] D. Xiao, L. Fang, Z. Liu, Y. He, J. Ying, H. Qin, A. Lu, M. Shi, T. Li, B. Zhang, J. Guan, C. Wang, Y. Abu-Amer, J. Shen, DNA methylation mediated Rbpjk suppression protects against fracture nonunion caused by systemic inflammation, J. Clin. Invest. 134 (3) (2023) e168558.

[3] D.J. Papachristou, S. Georgopoulos, P.V. Giannoudis, E. Panagiotopoulos, Insights into the cellular and molecular mechanisms that govern the fracture-healing process: a narrative review, J. Clin. Med. 10 (16) (2021) 3554.

[4] J. Loeffler, G.N. Duda, F.A. Sass, A. Dienelt, The metabolic microenvironment steers bone tissue regeneration, Trends Endocrinol. Metabol. 29 (2) (2018) 99–110.

[5] M. Maruyama, C. Rhee, T. Utsunomiya, N. Zhang, M. Ueno, Z. Yao, S.B. Goodman, Modulation of the inflammatory response and bone healing, Front. Endocrinol. 11 (2020) 386.

[6] Y. Liu, R. Xu, H. Gu, E. Zhang, J. Qu, W. Cao, X. Huang, H. Yan, J. He, Z. Cai, Metabolic reprogramming in macrophage responses, Biomark. Res. 9 (1) (2021) 1.

[7] E.L. Mills, D.G. Ryan, H.A. Prag, D. Dikovskaya, D. Menon, Z. Zaslona, M. P. Jedrychowski, A.S.H. Costa, M. Higgins, E. Hams, J. Szpyt, M.C. Runtsch, M. S. King, J.F. McGouran, R. Fischer, B.M. Kessler, A.F. McGettrick, M.M. Hughes, R. G. Carroll, L.M. Booty, E.V. Knatko, P.J. Meakin, M.L.J. Ashford, L.K. Modis, G. Brunori, D.C. Sevin, P.G. Fallon, S.T. Caldwell, E.R.S. Kunji, E.T. Chouchani, C. Frezza, A.T. Dinkova-Kostova, R.C. Hartley, M.P. Murphy, L.A. O'Neill, Itaconate is an anti-inflammatory metabolite that activates Nrf2 via alkylation of KEAP1, Nature 556 (7699) (2018) 113–117.

[8] C.G. Peace, L.A. O'Neill, The role of itaconate in host defense and inflammation, J. Clin. Invest. 132 (2) (2022) e148548.

[9] L.A.J. O'Neill, M.N. Artyomov, Itaconate: the poster child of metabolic reprogramming in macrophage function, Nat. Rev. Immunol. 19 (5) (2019) 273–281.

[10] Z. Zhu, Y. Lin, L. Li, K. Liu, W. Wen, S. Ding, M. Liu, L. Lu, C. Zhou, B. Luo, 3D printing drug-free scaffold with triple-effect combination induced by copper-doped layered double hydroxides for the treatment of bone defects, ACS Appl. Mater. Interfaces 15 (50) (2023) 58196–58211.

[11] P. Wang, Y. Yuan, K. Xu, H. Zhong, Y. Yang, S. Jin, K. Yang, X. Qi, Biological applications of copper-containing materials, Bioact. Mater. 6 (4) (2021) 916–927.

[12] C. Dong, W. Feng, W. Xu, L. Yu, H. Xiang, Y. Chen, J. Zhou, The coppery age: copper (Cu)-Involved nanotheranostics, Adv. Sci. 7 (21) (2020) 2001549.

[13] L. Zhang, G. Jiao, Y. You, X. Li, J. Liu, Z. Sun, Q. Li, Z. Dai, J. Ma, H. Zhou, G. Li, C. Meng, Y. Chen, Arginine methylation of PPP1CA by CARM1 regulates glucose metabolism and affects osteogenic differentiation and osteoclastic differentiation, Clin. Transl. Med. 13 (9) (2023) e1369.

[14] W. Zhan, J. Quan, Z. Chen, T. Liu, M. Deng, Z. Zhao, X. Wu, Z. Zhong, F. Gao, J. Chu, Toxoplasma gondii excretory/secretory proteins promotes osteogenic differentiation of bone marrow mesenchymal stem cells via aerobic glycolysis mediated by Wnt/beta-catenin signaling pathway, Int. J. Mol. Med. 52 (4) (2023) 91.

[15] J. Wu, M. Hu, H. Jiang, J. Ma, C. Xie, Z. Zhang, X. Zhou, J. Zhao, Z. Tao, Y. Meng, Z. Cai, T. Song, C. Zhang, R. Gao, C. Cai, H. Song, Y. Gao, T. Lin, C. Wang, X. Zhou, Endothelial cell-derived lactate triggers bone mesenchymal stem cell histone lactylation to attenuate osteoporosis, Adv. Sci. 10 (31) (2023) e2301300.

[16] S.C. Cheng, J. Quintin, R.A. Cramer, K.M. Shepardson, S. Saeed, V. Kumar, E. J. Giamarellos-Bourboulis, J.H. Martens, N.A. Rao, A. Aghajanirefah, G.R. Manjeri, Y. Li, D.C. Ifrim, R.J. Arts, B.M. van der Veer, P.M. Deen, C. Logie, L.A. O'Neill, P. Willems, F.L. van de Veerdonk, J.W. van der Meer, A. Ng, L.A. Joosten, C. Wijmenga, H.G. Stunnenberg, R.J. Xavier, M.G. Netea, mTOR- and HIF-1alpha-mediated aerobic glycolysis as metabolic basis for trained immunity, Science 345 (6204) (2014) 1250684.

[17] D. Kim, P.P. Khin, O.K. Lim, H.S. Jun, LPA/LPAR1 signaling induces PGAM1 expression via AKT/mTOR/HIF-1alpha pathway and increases aerobic glycolysis, contributing to keratinocyte proliferation, Life Sci. 311 (Pt B) (2022) 121201.

[18] M. Wagegg, T. Gaber, F.L. Lohanatha, M. Hahne, C. Strehl, M. Fangradt, C.L. Tran, K. Schonbeck, P. Hoff, A. Ode, C. Perka, G.N. Duda, F. Buttgereit, Hypoxia promotes osteogenesis but suppresses adipogenesis of human mesenchymal stromal cells in a hypoxia-inducible factor-1 dependent manner, PLoS One 7 (9) (2012) e46483.

[19] Y. Wu, B. Li, D. Yu, Z. Zhou, M. Shen, F. Jiang, CBX7 rejuvenates late passage dental pulp stem cells by maintaining stemness and pro-angiogenic ability, Tissue Eng. Regen. Med. 20 (3) (2023) 473–488.

[20] Z. Tan, B. Zhou, J. Zheng, Y. Huang, H. Zeng, L. Xue, D. Wang, Lithium and copper induce the osteogenesis-angiogenesis coupling of bone marrow mesenchymal stem cells via crosstalk between canonical wnt and HIF-1alpha signaling pathways, Stem Cell. Int. 2021 (2021) 6662164.

[21] M. Zhang, F. Xu, J. Cao, Q. Dou, J. Wang, J. Wang, L. Yang, W. Chen, Research advances of nanomaterials for the acceleration of fracture healing, Bioact. Mater. 31 (2024) 368–394.

[22] W. Ji, P. Zhang, G. Feng, Y.Z. Cheng, T.X. Wang, D. Yuan, R. Cha, X. Ding, S. Lei, B. H. Han, Synthesis of a covalent organic framework with hetero-environmental pores and its medicine co-delivery application, Nat. Commun. 14 (1) (2023) 6049.

[23] S. Bhunia, M.K. Jaiswal, K.A. Singh, K.A. Deo, A.K. Gaharwar, 2D covalent organic framework direct osteogenic differentiation of stem cells, Adv. Healthcare Mater. 11 (10) (2022) e2101737.

[24] S. Yue, H. He, B. Li, T. Hou, Hydrogel as a biomaterial for bone tissue engineering: a review, Nanomaterials 10 (8) (2020) 1511.

[25] C. Gao, W. Dai, X. Wang, L. Zhang, Y. Wang, Y. Huang, Z. Yuan, X. Zhang, Y. Yu, X. Yang, Q. Cai, Magnesium gradient-based hierarchical scaffold for dual-lineage regeneration of osteochondral defect, Adv. Funct. Mater. 33 (43) (2023) 2304829.

[26] L. Moradi, L. Witek, V. Vivekanand Nayak, A. Cabrera Pereira, E. Kim, J. Good, C. J. Liu, Injectable hydrogel for sustained delivery of progranulin derivative Atsttrin in treating diabetic fracture healing, Biomaterials 301 (2023) 122289.

[27] J. Li, S.S.Y. Leung, Y.L. Chung, S.K.H. Chow, V. Alt, M. Rupp, C. Brochhausen, C. S. Chui, M. Ip, W.H. Cheung, R.M.Y. Wong, Hydrogel delivery of DNase I and liposomal vancomycin to eradicate fracture-related methicillin-resistant staphylococcus aureus infection and support osteoporotic fracture healing, Acta Biomater. 164 (2023) 223–239.

[28] L. Chen, C. Yu, Y. Xiong, K. Chen, P. Liu, A.C. Panayi, X. Xiao, Q. Feng, B. Mi, G. Liu, Multifunctional hydrogel enhances bone regeneration through sustained release of Stromal Cell-Derived Factor-1alpha and exosomes, Bioact. Mater. 25 (2023) 460–471.

[29] X. Wang, W. Dai, C. Gao, L. Zhang, Z. Wan, T. Zhang, Y. Wang, Y. Tang, Y. Yu, X. Yang, Q. Cai, Spatiotemporal modulated scaffold for endogenous bone regeneration via harnessing sequentially released guiding signals, ACS Appl. Mater. Interfaces 15 (50) (2023) 58873–58887.

[30] B. Mi, Y. Xiong, L. Lu, J. Liao, G. Liu, Y. Zhao, Macrophage-mediated fracture healing: unraveling molecular mechanisms and therapeutic implications using hydrogel-based interventions, Biomaterials 305 (2024) 122461.

[31] B. Cai, D. Lin, Y. Li, L. Wang, J. Xie, T. Dai, F. Liu, M. Tang, L. Tian, Y. Yuan, L. Kong, S.G.F. Shen, N2-Polarized neutrophils guide bone mesenchymal stem cell recruitment and initiate bone regeneration: a missing piece of the bone regeneration puzzle, Adv. Sci. 8 (19) (2021) e2100584.

[32] D.G. Ryan, E.V. Knatko, A.M. Casey, J.L. Hukelmann, S. Dayalan Naidu, A. J. Brenes, T. Ekkunagul, C. Baker, M. Higgins, L. Tronci, E. Nikitopolou, T. Honda, R.C. Hartley, L.A.J. O'Neill, C. Frezza, A.I. Lamond, A.Y. Abramov, J.S.C. Arthur, D.A. Cantrell, M.P. Murphy, A.T. Dinkova-Kostova, Nrf2 activation reprograms macrophage intermediary metabolism and suppresses the type I interferon response, iScience 25 (2) (2022) 103827.

[33] Y. Zhang, Y. Gao, Y. Ding, Y. Jiang, H. Chen, Z. Zhan, X. Liu, Targeting KAT2A inhibits inflammatory macrophage activation and rheumatoid arthritis through epigenetic and metabolic reprogramming, MedComm (2020) 4 (3) (2023) e306.

[34] F. Liu, R. Han, S. Nie, Y. Cao, X. Zhang, F. Gao, Z. Wang, L. Xing, Z. Ouyang, L. Sui, W. Mi, X. Wu, L. Sun, M. Hu, D. Liu, Metformin rejuvenates Nap1l2-impaired immunomodulation of bone marrow mesenchymal stem cells via metabolic reprogramming, Cell Prolif. (2024) e13612.

[35] S. Ciliveri, A. Bandyopadhyay, Additively manufactured SiO(2) and Cu-added Ti implants for synergistic enhancement of bone formation and antibacterial efficacy, ACS Appl. Mater. Interfaces 16 (3) (2024) 3106–3115.

[36] K. Zheng, J. Wu, W. Li, D. Dippold, Y. Wan, A.R. Boccaccini, Incorporation of Cu-containing bioactive glass nanoparticles in gelatin-coated scaffolds enhances

bioactivity and osteogenic activity, ACS Biomater. Sci. Eng. 4 (5) (2018) 1546–1557.
[37] Q. Wu, S. Xu, X. Wang, B. Jia, Y. Han, Y. Zhuang, Y. Sun, Z. Sun, Y. Guo, H. Kou, C. Ning, K. Dai, Complementary and synergistic effects on osteogenic and angiogenic properties of copper-incorporated silicocarnotite bioceramic: in vitro and in vivo studies, Biomaterials 268 (2021) 120553.
[38] L. Pang, R. Zhao, J. Chen, J. Ding, X. Chen, W. Chai, X. Cui, X. Li, D. Wang, H. Pan, Osteogenic and anti-tumor Cu and Mn-doped borosilicate nanoparticles for syncretic bone repair and chemodynamic therapy in bone tumor treatment, Bioact. Mater. 12 (2022) 1–15.
[39] Y. Li, G. Zhong, T. He, J. Quan, S. Liu, Z. Liu, Z. Tang, W. Yu, Effect of arsenic and copper in kidney of mice: crosstalk between Nrf2/Keap1 pathway in apoptosis and pyroptosis, Ecotoxicol. Environ. Saf. 266 (2023) 115542.
[40] C.C. Zhong, T. Zhao, C. Hogstrand, F. Chen, C.C. Song, Z. Luo, Copper (Cu) induced changes of lipid metabolism through oxidative stress-mediated autophagy and Nrf2/PPARgamma pathways, J. Nutr. Biochem. 100 (2022) 108883.
[41] W. Xu, Y. Wang, G. Hou, J. Wang, T. Wang, J. Qian, A. Suo, Tumor microenvironment responsive hollow nanoplatform for triple amplification of oxidative stress to enhance cuproptosis-based synergistic cancer therapy, Adv. Healthcare Mater. 12 (13) (2023) e2202949.
[42] L. Xu, J. Cai, C. Li, M. Yang, T. Duan, Q. Zhao, Y. Xi, L. Sun, L. He, C. Tang, L. Sun, 4-Octyl itaconate attenuates LPS-induced acute kidney injury by activating Nrf2 and inhibiting STAT3 signaling, Mol. Med. 29 (1) (2023) 58.
[43] P. Zhang, Y. Wang, W. Yang, Y. Yin, C. Li, X. Ma, L. Shi, R. Li, K. Tao, 4-Octyl itaconate regulates immune balance by activating Nrf2 and negatively regulating PD-L1 in a mouse model of sepsis, Int. J. Biol. Sci. 18 (16) (2022) 6189–6209.
[44] H. Xiao, Y. Dong, D. Wan, J. Wan, J. Huang, L. Tang, J. Zhou, T. Yang, Y. Liu, S. Wang, Injectable hydrogel loaded with 4-octyl itaconate enhances cartilage regeneration by regulating macrophage polarization, Biomater. Sci. 11 (7) (2023) 2445–2460.
[45] X. Chu, L. Li, W. Yan, H. Ma, 4-Octyl itaconate prevents free fatty acid-induced lipid metabolism disorder through activating nrf2-AMPK signaling pathway in hepatocytes, Oxid. Med. Cell. Longev. 2022 (2022) 5180242.
[46] S.Y. Park, H.J. Lee, J.H. Song, Y.K. Shin, A.M. Abd El-Aty, A. Ramadan, A. Hacimuftuoglu, J.H. Jeong, T.W. Jung, Dimethyl itaconate attenuates palmitate-induced insulin resistance in skeletal muscle cells through the AMPK/FGF21/PPARdelta-mediated suppression of inflammation, Life Sci. 287 (2021) 120129.
[47] L. Li, Z. Cui, H. Wang, B. Huang, H. Ma, Dietary supplementation of dimethyl itaconate protects against chronic heat stress-induced growth performance impairment and lipid metabolism disorder in broiler chickens, J. Anim. Sci. 101 (2023).
[48] W.R. Cui, C.R. Zhang, W. Jiang, R.P. Liang, J.D. Qiu, Covalent organic framework nanosheets for fluorescence sensing via metal coordination, ACS Appl. Nano Mater. 2 (8) (2019) 5342–5349.